

# Sol–gel Synthesis of Kaolin/TiO<sub>2</sub> Nanocomposites for Photocatalytic Degradation of Tannery Wastewater



S. Mustapha, J. O. Tijani, T. C. Egbosiuba, A. Sumaila, T. A. Amigun, A. B. Salihu, Y. O. Ibrahim, M. M. Ndamitso, and S. A. Abdulkareem

**Abstract** In this study, a TiO<sub>2</sub> immobilized on kaolin was synthesized by the sol–gel route. The surface morphology, chemical and phase composition of the kaolin, synthesized TiO<sub>2</sub> nanoparticles, and their nanocomposites were investigated using high-resolution scanning electron microscopy (HRSEM), RAMAN spectroscopy, high-resolution transmission electron microscopy (HRTEM) coupled with energy dispersive spectroscopy (EDX) and selected area electron diffraction (SAED). The influence of operational parameters such as irradiation time and catalyst dosage were evaluated. The influence of irradiation light on the degradation of chemical oxygen demand (COD) and total organic carbon (TOC) in tannery wastewater was found to be highest in 90 min, which follows a linear removal efficiency. It was evident that the photocatalytic degradation rate initially increases with catalyst loading and then decreases at high values. Almost complete decolourization was obtained upon 90 min of sunlight irradiation in the presence of kaolin/TiO<sub>2</sub> catalyst. The satisfactory stability in recyclability of photocatalyst indicates colour, COD and TOC abatement in tannery wastewater treatment. It is clear that photocatalysis has good potential to degrade organic pollutants. Thus, there is a need to determine the degradability performance on a commercial scale.

---

S. Mustapha (✉) · J. O. Tijani · A. Sumaila · M. M. Ndamitso  
Department of Chemistry, Federal University of Technology, PMB 65, Bosso Campus, Minna, Nigeria

S. A. Abdulkareem  
Department of Chemical Engineering, Federal University of Technology, PMB 65, Gidan Kwano Campus, Minna, Niger State, Nigeria

S. Mustapha · J. O. Tijani · T. C. Egbosiuba · A. Sumaila · Y. O. Ibrahim · M. M. Ndamitso · S. A. Abdulkareem  
Nanotechnology Research Group, Africa Center of Excellence for Mycotoxin and Food Safety, Federal University of Technology, PMB 65, Minna, Niger State, Nigeria

T. A. Amigun  
Department of Chemical and Geological Sciences, Al-Hikmah University, Ilorin, Nigeria

A. B. Salihu  
Department of Chemical Sciences, Federal Polytechnic, Bida, Niger State, Nigeria

**Keywords** Immobilized · Synthesized · Operational parameter · Catalyst dosage · Organic pollutants

## 1 Introduction

Water pollution is one of the most concerning human health and sustainability challenges. Industrial sectors are principally responsible for thousands of organic and inorganic contaminants associated with wastewater released worldwide. These unregulated contaminants comprise pharmaceuticals, herbicides, and heavy metals. Organic and inorganic substances discharged from many industries such as metal plating, tanneries, mining, smelting, food processing, battery and smelting industries do not degrade into harmless end products, thus causing threats to humans and the environment (Engwa et al. 2019; Dehghani et al. 2021; Karri et al. 2021).

Various treatment technologies have been used to remove heavy metals from wastewater. These methods include coagulation/flocculation, ozonation, membrane filtration, photocatalyst, precipitation, and ion exchange (Crini and Lichtfouse 2019). Besides, most of these methods have their advantages and limitations in terms of capital cost, efficiency and operational conditions. However, the adsorption technique has been proposed as an alternative measure for removing heavy metals from wastewater (Nabbou et al. 2019; Khan et al. 2021; Mehmood et al. 2021; Lingamdinne et al. 2022). This method is considered to be simple, promising and effective for wastewater treatment due to its high adsorption capacity and insensitivity to heavy metals.

Nowadays, adsorbents like zeolites, activated carbon, nanoparticles, clay minerals and others are used for wastewater treatment. Currently, nanoparticles have received huge attention in treating wastewater globally (Mehmood et al. 2021). Some limitations in using these nanoparticles are the low adsorption capacity of hydrophobic pollutants related to its low surface area affecting the removal efficiency of contaminants. Other related issues of nanoparticles application in wastewater treatment are particle agglomeration and formation of suspension in water. Other practical problems are catalyst agglomeration and the formation of uniform suspension in water which makes it difficult to separate. This implies that removing these nanoparticles could require costly phase separation methods. It was reported by Mahvi et al. (2009) that the separation and recovery of  $\text{TiO}_2$  nanoparticles from treated wastewater are expensive and time-consuming. They concluded that the depth of UV penetration was reduced due to strong absorption between  $\text{TiO}_2$  and dye solution, and this problem could be solved by anchoring  $\text{TiO}_2$  nanoparticles on the surface of the support adsorbent. But if these nanoparticles are embedded in clay minerals such as kaolin, bentonite and montmorillonite, the environmental problems will be reduced. Clay minerals are highly porous materials with a large surface area for physical and chemical reactions on their surfaces (Boruah et al. 2019). Therefore, their applications in adsorption processes are essential. Owing to these aforementioned merits, the interaction of nanoparticles with clay minerals will be of interest in solving separation problems of nanoparticles in water.

Furthermore, it is expected that the photocatalytic oxides coupled with clay favoured the photocatalyst via reduction of the bandgap due to the closeness oxides. Thus, the mechanical properties of photocatalyst enhance the photodegradation of pollutants in an aqueous solution (Silvestri and Foletto 2017; Ahmed et al. 2021). Various research articles reported the use of nanoparticles-clay composites to remove contaminants from wastewater (Mehmood et al. 2021). Among the studies carried out were the adsorption of methylene blue (MB) using titanium oxide/tungsten oxide/bentonite nanocomposites (Yang et al. 2015), synthesized clay/titanium oxide for the removal of lead, cadmium, copper and zinc ions from aqueous solution (Dukic et al. 2015), the use of titanium oxide/clay composites for removal of MB and cadmium ion (Aliou et al. 2018), the adsorption and photodegradation activities of titanium oxide/bentonite on the removal of dyes (Laysandr et al. 2017) and the photocatalytic effect using dyes on synthesized titanium oxide/clay nanocomposites (Mishra et al. 2017). To the best of our information, the photocatalysis application of kaolin as support to immobilized titanium oxide for the removal of total organic carbon (TOC) and chemical oxygen demand (COD) from tannery wastewater is scarce in the literature. In this present study, kaolin, TiO<sub>2</sub> and kaolin/TiO<sub>2</sub> were characterized by morphology, optical and structural properties. In addition, the influence of parameters such as time and catalyst dosage, the point of zero change effect on kaolin, TiO<sub>2</sub> and kaolin/TiO<sub>2</sub> and the effect of the photocatalytic properties in decolourization of tannery wastewater under sunlight have been demonstrated.

## 2 Materials and Methods

### 2.1 Materials

Raw kaolin was obtained from a clay deposit in Gbako Local Government Area in Niger State, Nigeria. The collected tannery wastewater from Majema Tannery industry, Manuri Road, Tudun Wada Area, Sokoto State was characterized for chemical oxygen demand (COD) using the method as described by the American Public Health Association (APHA) (2017), while total organic carbon (TOC) was determined using a TOC analyzer (model, Shimadzu, 5050A). Titanium tetraisopropoxide (TTIP, 97%), sodium hydroxide (NaOH,  $\geq 97\%$ ), hydrochloric acid (HCl, 37%), and hydrogen peroxide (H<sub>2</sub>O<sub>2</sub>) were procured from Sigma Aldrich. All the reagents were analytical grade.

### 2.2 Kaolin Preparation

Exactly 20.0 g raw kaolin sample was weighed in a 250 cm<sup>3</sup> beaker containing 5 cm<sup>3</sup> H<sub>2</sub>O<sub>2</sub>, which acts as a bleaching agent and 20 cm<sup>3</sup> of 1.0 M HCl to dissolve

undesirable soluble contents. The mixture was stirred with a glass rod for some time and allowed to stand for 12 h. Solution of three layers (water, finer particles and fine particles) was formed. The first and second layers (water and finer particles) were decanted from the solution into a separate 250 cm<sup>3</sup> beaker, washed with de-ionized water many times until neutral (pH 7). The kaolin paste was dried at 105 °C for 5 h to evaporate the water and calcined at 450 °C for 3 h, crushed with mortar and pestle.

### **2.3 *TiO<sub>2</sub> Nanoparticle Preparation***

TiO<sub>2</sub> nanoparticles were prepared using the sol–gel method. A 5 cm<sup>3</sup> of titanium isopropoxide was measured, added to 50 cm<sup>3</sup> of de-ionized water in a 250 cm<sup>3</sup> beaker and then stirred at 180 rpm for 1 h. The resultant mixture was adjusted to pH 7 using 0.1 M aqueous NaOH solution with continuous magnetic stirring at 180 rpm for 3 h. The mixture was washed copiously with de-ionized water to remove free ions, dried at 105 °C in an oven for 12 h, crushed and calcined at 450 °C for 3 h.

### **2.4 *TiO<sub>2</sub>/Kaolin Preparation***

A 5.0 g beneficiated kaolin was weighed in a 200 cm<sup>3</sup> beaker, and 50 cm<sup>3</sup> of ionized water was stirred at 180 rpm for 30 min, and 1 cm<sup>3</sup> of TTIP was added to the stirred kaolin suspension. The resultant kaolin/TiO<sub>2</sub> was adjusted until pH 7 and washed with de-ionized water to remove free soluble ions. The wet composite kaolin/TiO<sub>2</sub> was dried in an oven at 105 °C for 3 h and stored for catalysis.

### **2.5 *Point of Zero Charge***

The pH<sub>pzc</sub> values for kaolin, TiO<sub>2</sub> and kaolin/TiO<sub>2</sub> were determined. Exactly 50 cm<sup>3</sup> of 0.05 M HCl and 0.05 M NaOH solutions were added to kaolin (0.20 g), TiO<sub>2</sub> (0.20 g) and kaolin/TiO<sub>2</sub> (0.20 g) each for adjustment of pH values (2, 4, 6, 8, 10 and 12) at 25 °C prepared in three sets of six 250 cm<sup>3</sup> conical flasks. The conical flasks were shaken using a rotary shaker at 200 rpm for 6 h. The dispersed samples were allowed to settle, and their final pH was determined.

### **2.6 *Photocatalytic Study***

The photocatalysis activities were performed under direct sunlight. A 100 cm<sup>3</sup> of tannery wastewater was measured in a 250 cm<sup>3</sup> beaker, 0.2 g of kaolin/TiO<sub>2</sub> catalyst

was introduced, and then placed under high-intensity sunlight. At different irradiation time intervals, samples were collected and analyzed using UV-visible spectroscopy. The removal efficiency of COD and TOC is expressed as follows:

$$\text{Removal efficiency}(E_r) = \frac{C_o - C_t}{C_o} \times 100 \quad (1)$$

where  $C_o$  and  $C_t$  are the initial concentration of pollutants and residual concentration of COD and TOC at different intervals of irradiation (0–150 min).

The extent of reusability of the kaolin/TiO<sub>2</sub> photocatalyst was determined in six consecutive experimental runs using deionized water several times until pH 7 was attained and dried at 105 °C for 12 h.

## 2.7 Characterization Techniques

The composition of kaolin, TiO<sub>2</sub> and kaolin/TiO<sub>2</sub> were determined by high-resolution scanning electron microscopy coupled with energy dispersive spectroscopy (HRSEM), RAMAN spectroscopy, UV-visible spectrophotometer, high-resolution transmission electron microscopy (HRTEM). The morphology of the samples was examined with HRTEM, a Zeiss Auriga model (USA) operated at a 20 kV of voltage, while HRTEM coupled with energy dispersed spectroscopy (EDX) was performed using a Zeiss Auriga model (USA) at an accelerating voltage of 20 kV. Raman spectroscopy was recorded at an ambient temperature in the wavenumber range of 300–2000 cm<sup>-1</sup>. The UV-visible absorption spectra of the samples were examined using a UV-visible spectrophotometer, Shimadzu UV 1800.

## 3 Discussion

### 3.1 Characterization

The surface morphology of beneficiated kaolin was presented by HRSEM as seen in Plate 1a. The HRSEM image confirmed kaolin's hexagonal plates and stack appearance (see Fig. 1a). Also, the HRSEM image of kaolin revealed the large blocked and small pieces of kaolinite structure. The morphology of the synthesized TiO<sub>2</sub> nanoparticles calcined at 450 °C was characterized by HRSEM as presented in Fig. 1b. The anatase phase of TiO<sub>2</sub> nanoparticles exhibited agglomerated spherical shapes with an average size distribution of 14 nm. However, the discernable pores structure at the space between the TiO<sub>2</sub> nanoparticles is revealed at the surface of the synthesized particles. In Plate 1c, the HRSEM micrograph of kaolin/TiO<sub>2</sub> nanocomposites revealed a dispersed and block structure of TiO<sub>2</sub> nanoparticles on the surface.

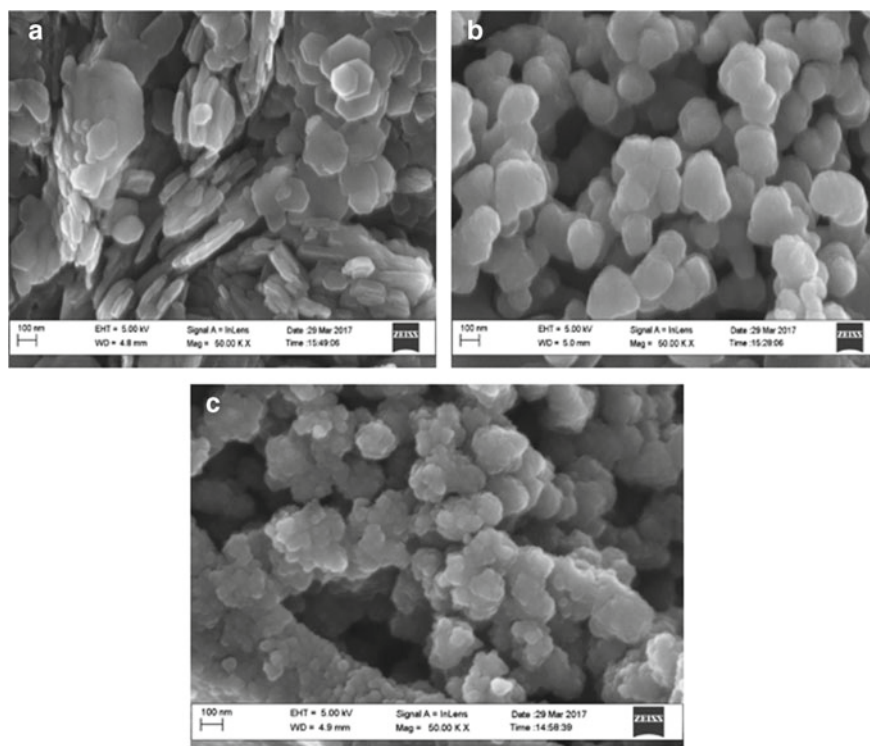


**Fig. 1** HRSEM images of **a** beneficiated kaolin **b**  $\text{TiO}_2$  nanoparticles and **c** kaolin/ $\text{TiO}_2$  nanocomposites at  $450^\circ\text{C}$

The microstructure of kaolin was characterized by HRTEM and revealed a pseudo-hexagonal structure of kaolinite, as shown in Plate 2a. The EDX elemental analysis of kaolin was investigated. As shown in Fig. 2, O, Al, Si, Ti and Fe elements are apparently detected. The experimental percentage weight of O (54.96%), Al (19.84%) and Si (21.40%) from the EDX result are closely related to the percentage elemental composition of the theoretical structural formula of kaolin. The SAED result on the kaolin revealed the turbostratic arrangement of kaolinite oriented to one another (as seen in Fig. 3). The HRTEM structure of  $\text{TiO}_2$  nanoparticles calcined at  $450^\circ\text{C}$  was presented in Fig. 2. It was revealed that the nanoparticles consist of a spherical like appearance with a size of 13.8 nm, in accordance with the HRSEM result. As seen in the HRTEM image (Fig. 2b), lattice fringes of anatase (0.346 nm), corresponding to the (101) plane, were evaluated.

Additionally, the EDX results of  $\text{TiO}_2$  nanoparticles show the presence of dominant elements (Ti and O). The spectrum showed sharp peaks corresponding to Ti at 4.72 and 4.94 keV. The observed small peaks of Ni could be related to impurities. The SAED analysis as displayed in Plate 2b showed that the  $\text{TiO}_2$  nanoparticles are

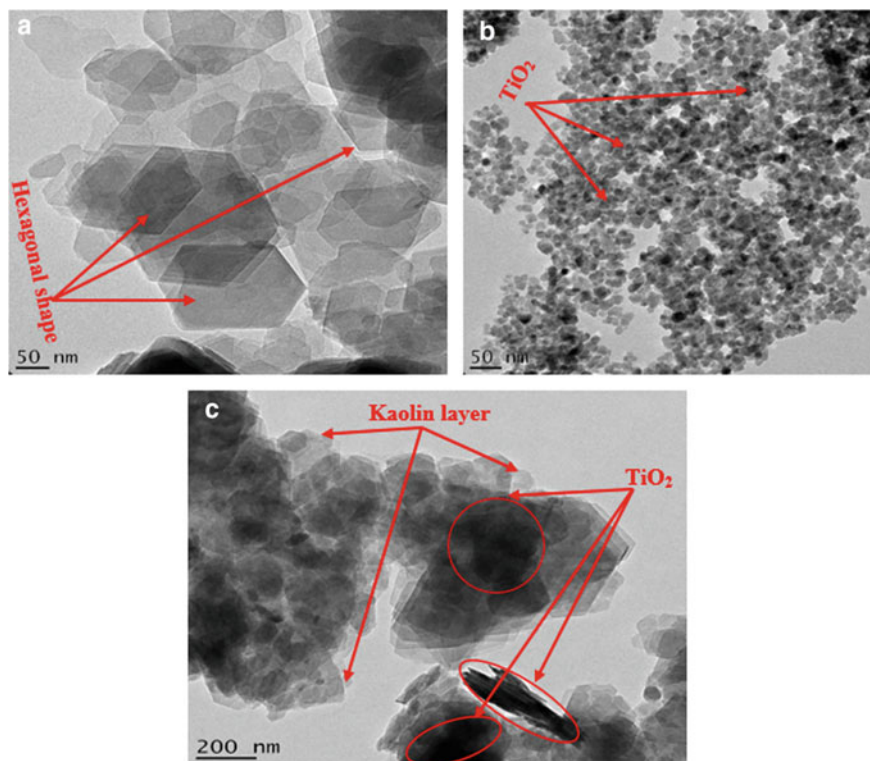


**Fig. 2** HRTEM images of **a** beneficiated kaolin **b** TiO<sub>2</sub> nanoparticles and **c** kaolin/TiO<sub>2</sub> nanocomposites at 450 °C

crystalline with dotted concentric rings. TiO<sub>2</sub>/kaolin nanocomposites were characterized by HRTEM microscopy. The image Fig. 2c showed the presence of layered kaolin and the elongated appearance of TiO<sub>2</sub> nanoparticles, indicating the embedment in the nanocomposites. The image displayed spherical TiO<sub>2</sub> nanoparticles, which showed lattice spacing of 0.35 and 0.24 nm characteristic of the (101) and (111) planes of the anatase phase. EDX analysis was performed to study the composition of the TiO<sub>2</sub>/kaolin nanocomposites (Fig. 4), indicating the presence of C, O, Al, Si, Ti, Fe and Cu. However, the peaks of C is from the carbon holey grid used for the HRTEM study and besides Cu from impurities. The selected area of electron diffraction (SAED) analysis indicates that the nanocomposites are crystalline in nature (Fig. 5).

Kaolin has an intense peak at 472.46 cm<sup>-1</sup> related to the observed less intense peak for kaolin/TiO<sub>2</sub>, whereas TiO<sub>2</sub> and kaolin/TiO<sub>2</sub> had similar significant vibration mode located at 367.19 and 512.41 cm<sup>-1</sup> (see Fig. 6). The band (472.46 cm<sup>-1</sup>) is attributed to the bending mode of Si-O-Al (Rodrigues et al. 2016). The peak of kaolin/TiO<sub>2</sub>

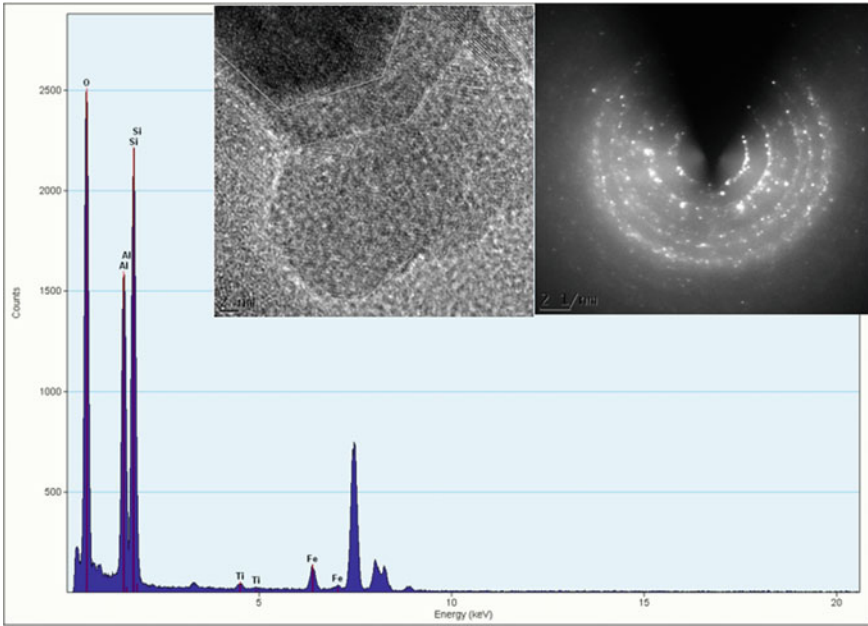


Fig. 3 EDX and SAED results for kaolin

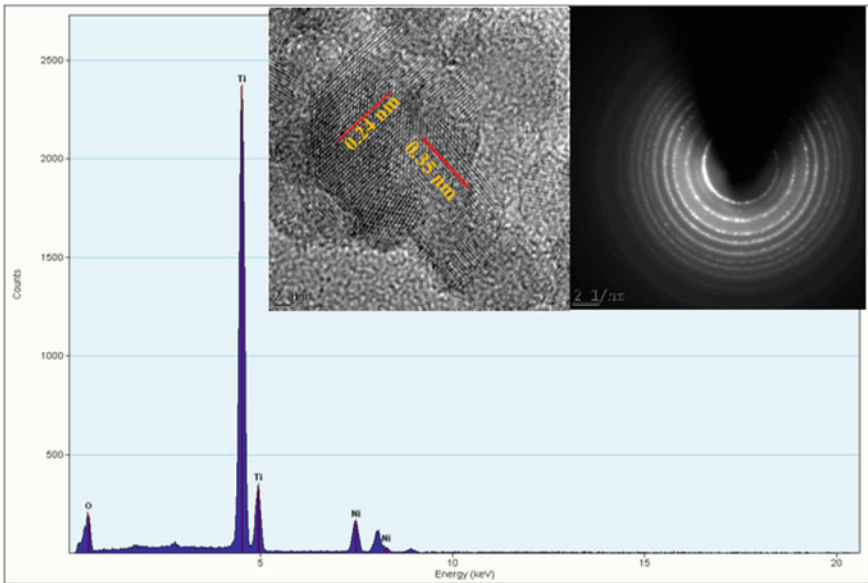


Fig. 4 EDX and SAED results for TiO<sub>2</sub> nanoparticles



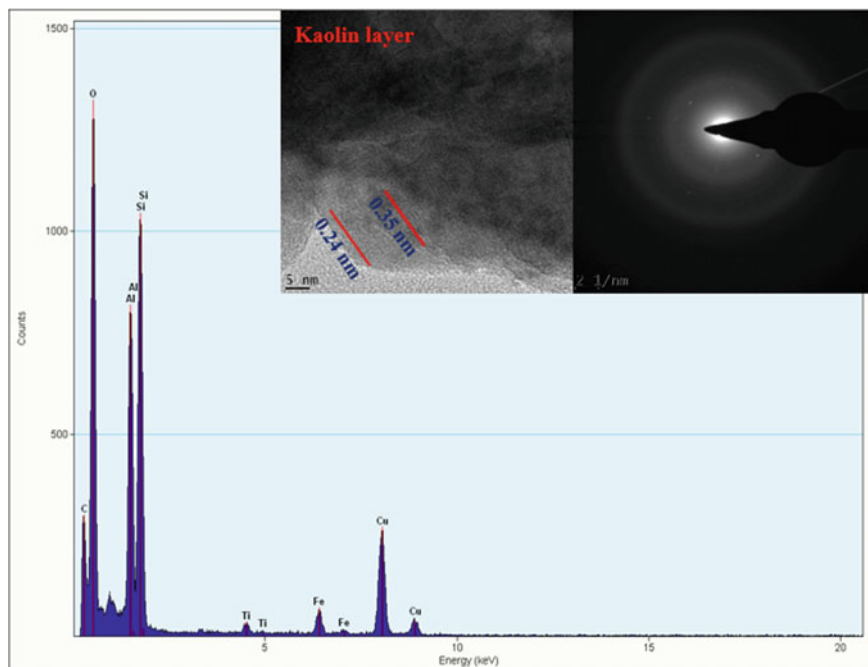


Fig. 5 EDX and SAED results for kaolin/TiO<sub>2</sub> nanocomposites

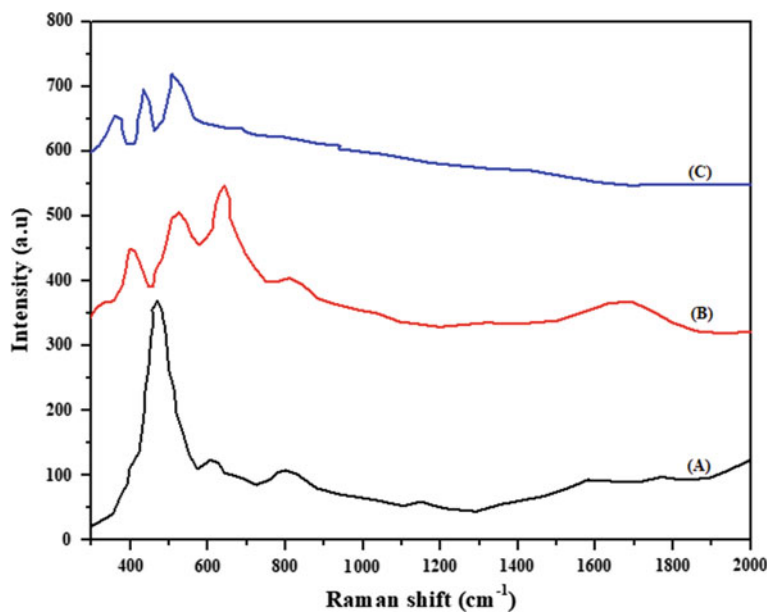


Fig. 6 The Raman spectra of kaolin, TiO<sub>2</sub> and kaolin/TiO<sub>2</sub>

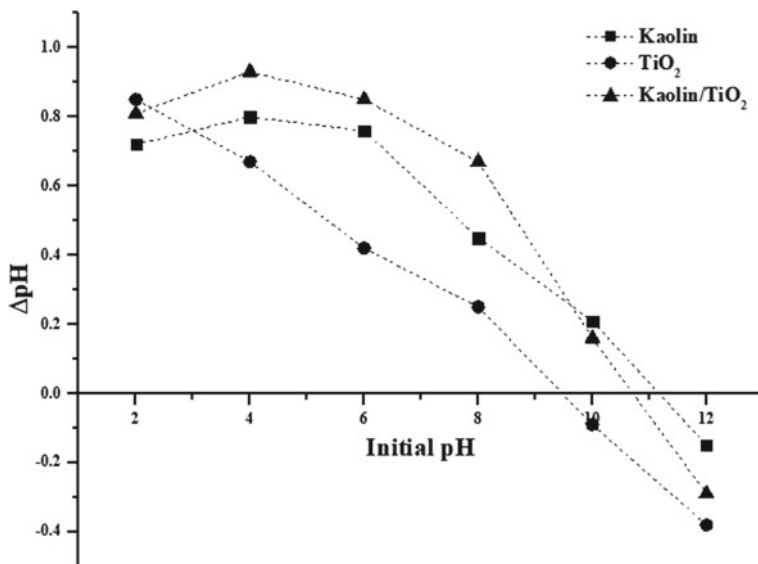


Fig. 7 Point of zero charge of kaolin, TiO<sub>2</sub> and kaolin/TiO<sub>2</sub>

(512.41 cm<sup>-1</sup>) indicated well-formed crystalline TiO<sub>2</sub> nanoparticles in the nanocomposites. The formation of peaks of TiO<sub>2</sub> nanoparticles in the nanocomposites was consistent with the TiO<sub>2</sub> structure.

#### Point of zero charge

The plots of change in pH against initial pH for kaolin, TiO<sub>2</sub> and kaolin/TiO<sub>2</sub> materials were depicted in Fig. 7. The kaolin revealed 11.09 pH<sub>pzc</sub>, which is positive at pH 2–10.5, and negative at pH higher than the (pH<sub>pzc</sub>). Figure 7 showed that the pure TiO<sub>2</sub> exhibited a positive surface charge at pH (9.44) lower than pH<sub>pzc</sub> of kaolin, where it becomes a negatively charged surface below the pH<sub>pzc</sub>. This indicated that the surface charge increased as the pH reduced. The kaolin/TiO<sub>2</sub> nanocomposites exhibited a pH<sub>pzc</sub> of 10.72, and that the surface was positively charged below pH values of 10 and negatively charged surface at pH greater than 10.7. The positive charges of the kaolin, TiO<sub>2</sub> and kaolin/TiO<sub>2</sub> surfaces are believed to be responsible for contamination photodegradation of radicals in tannery wastewater. At greater pH<sub>pzc</sub>, the negatively charged species in the wastewater would be repelled by the negatively charged kaolin, TiO<sub>2</sub> and kaolin/TiO<sub>2</sub> surfaces. This enables the contaminant species farther away from radicals, thus suggesting the photodegradation process become retarded at higher pH.

#### Effect of operational conditions

The efficient photocatalytic removal of TOC and COD under the influence of irradiation time and catalyst dosage was investigated.

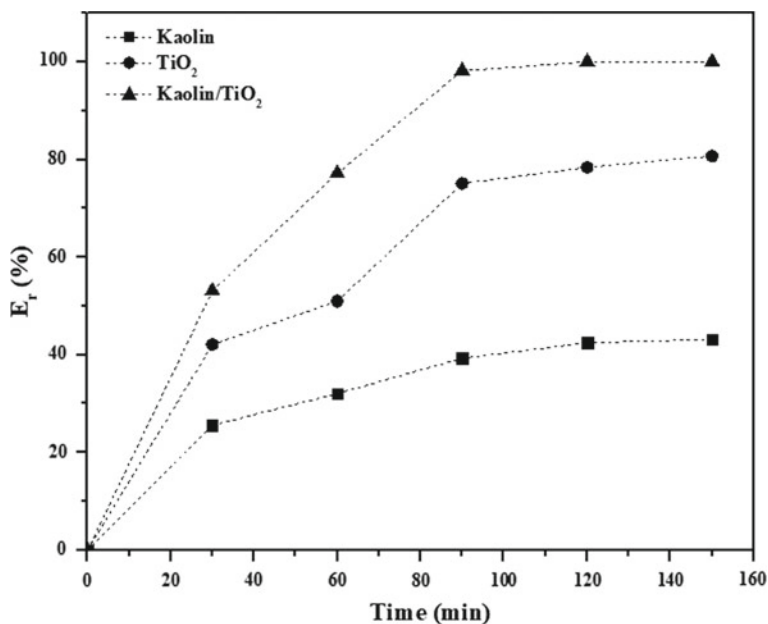


**Fig. 8** Effect of time on photocatalytic removal of TOC in tannery wastewater using kaolin, TiO<sub>2</sub> and kaolin/TiO<sub>2</sub> (Dosage = 0.2 g, pH = and Temperature = 28 °C)

#### *Effect of time*

COD and TOC experiments' removal efficiency was performed at 0.20 g of the kaolin, TiO<sub>2</sub> and kaolin/TiO<sub>2</sub>, each under sunlight at a different interval time (0 to 150 min) as depicted in Figs. 8 and 9. It was noticed that the removal efficiencies of the pollutants increase with time. After 90 and 120 min of reaction (maximal time), removal efficiency reached 100% compared to lower removal efficacies of kaolin and TiO<sub>2</sub>. Furthermore, it can be seen from Figs. 8 and 9 that removal efficiencies of the sample n followed the trend: kaolin/TiO<sub>2</sub> > TiO<sub>2</sub> > kaolin, confirming that TiO<sub>2</sub> loaded improved the photocatalytic activity of kaolin/TiO<sub>2</sub>.

#### *Effect of catalyst dosage*

The effect of time on the photodegradation of COD and TOC in tannery wastewater using kaolin, TiO<sub>2</sub> and kaolin/TiO<sub>2</sub> investigated over the range of 0.2 to 0.4 g are depicted in Figs. 10 and 11, respectively. An increase in dose and optimal dose with the maxima degradation of pollutant occurred. The results indicated that the removal efficiencies increase at constant concentrations of the pollutants by varying the adsorbent. The increase in removal efficiency could be attributed to the increased number of sites and available binding sites. It is noticed that the optimal dose, 0.40 g (100%), of the kaolin/TiO<sub>2</sub> photocatalyst is not far from that of 0.35 g (99.20%). This may have occurred due to the aggregation of adsorbent particles and repulsive force among the binding sites, leading to an increase in the binding sites.

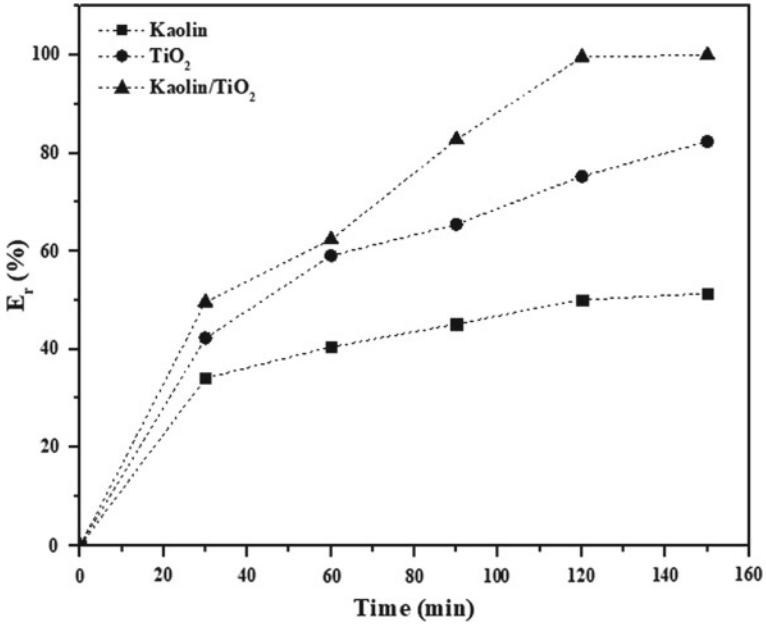


Fig. 9 Effect of time on photocatalytic removal of BOD in tannery wastewater using kaolin, TiO<sub>2</sub> and kaolin/TiO<sub>2</sub> (Dosage = 0.2 g, pH = and Temperature = 28 °C)

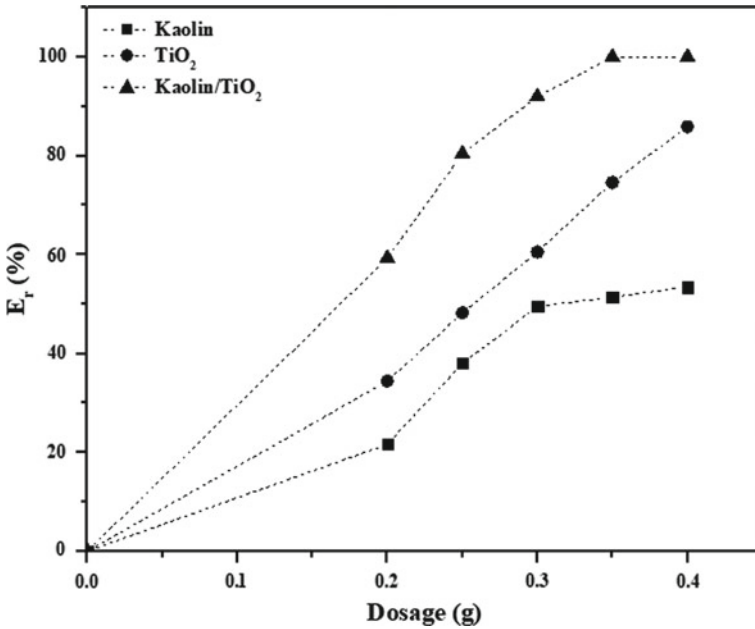
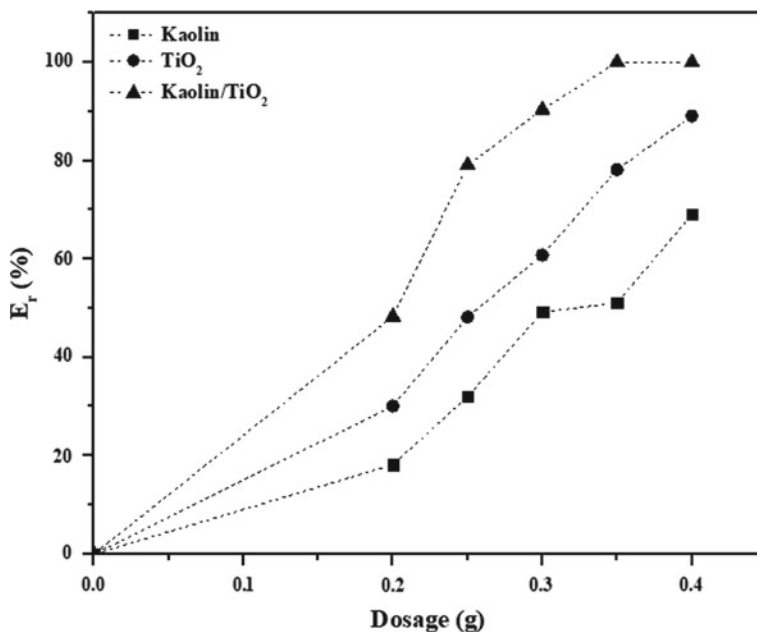


Fig. 10 Effect of dosage on photocatalytic removal of TOC in tannery wastewater using kaolin, TiO<sub>2</sub> and kaolin/TiO<sub>2</sub> (Time = 90 min, pH = and Temperature = 28 °C)



**Fig. 11** Effect of dosage on photocatalytic removal of BOD in tannery wastewater using kaolin, TiO<sub>2</sub> and kaolin/TiO<sub>2</sub> (Time = 90 min, pH = and Temperature = 28 °C)

#### *Discolourization of tannery wastewater*

UV-visible absorption spectra of the tannery wastewater solution with kaolin, TiO<sub>2</sub> and kaolin/TiO<sub>2</sub> at a different time using  $\lambda_{max}$  are presented in Fig. 12. The % decolourization of tannery wastewater was performed at pH 8.4, 0.2 g of kaolin/TiO<sub>2</sub> photocatalyst and 50 cm<sup>3</sup> of wastewater solution. The initial peaks of tannery wastewater decreased gradually by adding kaolin/TiO<sub>2</sub> and became smaller as time increased (30 to 90 min). The reduction of absorbance intensity of the sample showed the photodegradation of the wastewater under these conditions leading to the percentage reduction of COD and TOC. The percentage decolourization, 62.10% at 30 min, 75.50% at 60 min and 98.90% at 90 min, were achieved, corresponding to percentage reduction of COD and TOC. In this case, photodegradation was restricted to visible sunlight. At this point, the solution almost becomes colourless. The degradation of these pollutants confirmed the ability of TiO<sub>2</sub> nanoparticles, which enhanced photocatalytic efficiency by absorbing pollutants. A comparison between the present work and previous studies regarding the photodegradation of pollutants is presented in Table 1. The comparative study showed the efficacy of kaolin/TiO<sub>2</sub> for decolourization, TOC and BOD removal in real effluent (tannery wastewater). As it can be seen, the obtained maximum tannery wastewater discolourization was more favourable than most reported catalysts.

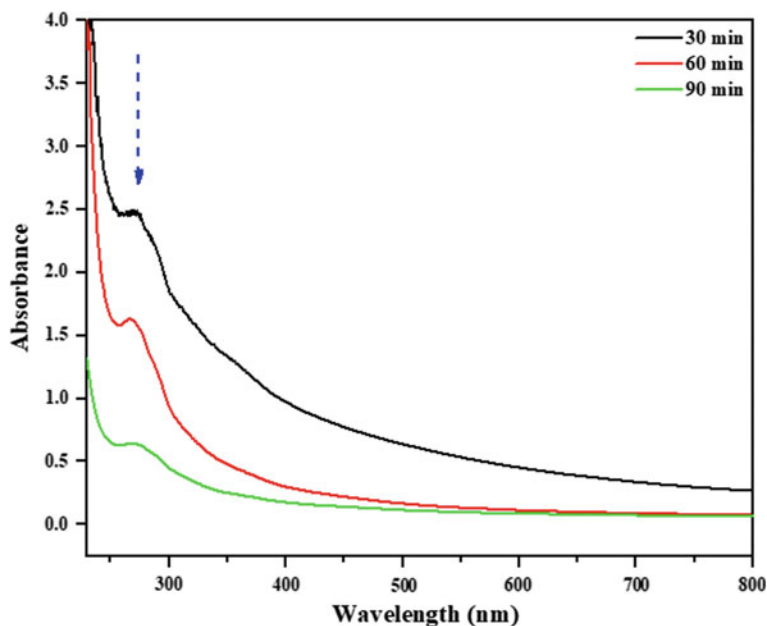


Fig. 12 Decolourization efficiency of tannery wastewater

The photocatalytic activity of kaolin/TiO<sub>2</sub> photocatalyst is related to the holes induced by releasing the electron from valance band to conduction band under UV light, as presented in Fig. 13. The conduction band electron decreased oxygen molecules produce superoxide radicals, and holes generated react with hydroxyl radicals. These forms of radicals serve as strong oxidative agents that degrade organic molecules.

During the interaction of kaolin/TiO<sub>2</sub> nanocomposites with tannery wastewater under sunlight, as depicted in Fig. 13, the photodegradation of pollutants involves adsorption of the photon, oxygen adsorption by the generation of superoxide radicals, generation of hydrogen atoms via photoelectrons, the yield of hydroxyl radicals and conversion of organic molecules by oxidation through hydroxyl radical attack. This result revealed that the photoactivity of kaolin/TiO<sub>2</sub> was due to the abundant surface oxygen vacancy and defects and the lower recombination of electron-hole of TiO<sub>2</sub> nanoparticles (Wang et al. 2011).

#### *Kinetic study.*

The kinetics of tannery wastewater using kaolin/TiO<sub>2</sub> photocatalyst were investigated by first-order model expression as follow:

$$\ln \frac{C_0}{C_t} = k_{app} t \quad (2)$$

**Table 1** Comparison of pollutant removal with literature

Adsorbent	Experimental conditions	Characterization	Pollutant removal	Rate ( $k_{app}$ )	Wastewater	Reference
TiO <sub>2</sub> /Clay	Oxidating agent, concentration, time	BET, FTIR, XRD, TGA/DTA, SEM	Decolourization = 100% at 20 min COD = 98% at 45 min		Reactive blue 19	Hadjilataief et al. (2019)
ZnO/Clay	pH, catalyst, dosage, concentration, time	XRD, FTIR, BET, SEM, HRTEM-EDX	Decolourization = 97.18% at 60 min for MG, 100% at 70 min for CR	CR = 0.0146 min <sup>-1</sup> MG = 0.0219 min <sup>-1</sup>	Malachite green (MG) Congo red (CR)	Hadjilataief et al. (2018)
Fungal biomass/TiO <sub>2</sub> /UV	Time, dosage	SEM-EDX	Decolourization = 89% at 6 h COD = 73% at 6 h BOD = 86% at 6 h		Textile effluent	Blanco-Vargas et al. (2018)
Porous ceramic/TiO <sub>2</sub>	Time dosage	XRD, RAMAN, SEM	Decolourization = 83% at 5 h	0.00627 min <sup>-1</sup>	Rhodamine B	De Araujo-Scharnberg et al. (2020)
Polyaniline/TiO <sub>2</sub>	Time, pH	FE-SEM, TEM, FTIR, TG	Decolourization = 84% at 90 min		Azo dye	Gilja et al. (2017)
TiO <sub>2</sub> /TPPS	Time, dosage	XRD, FTIR, SEM-EDX, UV-DRS	Decolourization = 99% at 50 min	0.0896 min <sup>-1</sup>	Eosin yellow dye	Manivannan et al. (2021)
TiO <sub>2</sub> /Fe <sub>2</sub> O <sub>3</sub>	Time	XRD, FE-SEM, PSD, XRF, XPS, DRS, BET	Decolourization = 64% at 540 min		Methylene blue	Retamoso et al. (2019)
Fe <sub>2</sub> O <sub>3</sub> /TiO <sub>2</sub> /Clay	Time, pH, concentration	XRD, XRF, BET, SEM-EDX, DRS	Decolourization = 91% at 45 min		Acid orange 7 dye	Silvestri and Feletto (2017)
Biochar/TiO <sub>2</sub>		XRD, SEM, BET, FTIR			Methylene blue	Silvestri et al. (2020)

(continued)

**Table 1** (continued)

Adsorbent	Experimental conditions	Characterization	Pollutant removal	Rate ( $k_{app}$ )	Wastewater	Reference
Kaolin/TiO <sub>2</sub>	Time, dosage	HRSEM, HRTEM-EDX, RAMAN, UV-visible,	Decolourization = 98.90% at 90 min COD = 100% at 90 min TOC = 100% at 90 min	TOC - 0.03221 min <sup>-1</sup> BOD = 0.0346 min <sup>-1</sup>	Tannery effluent	In this work



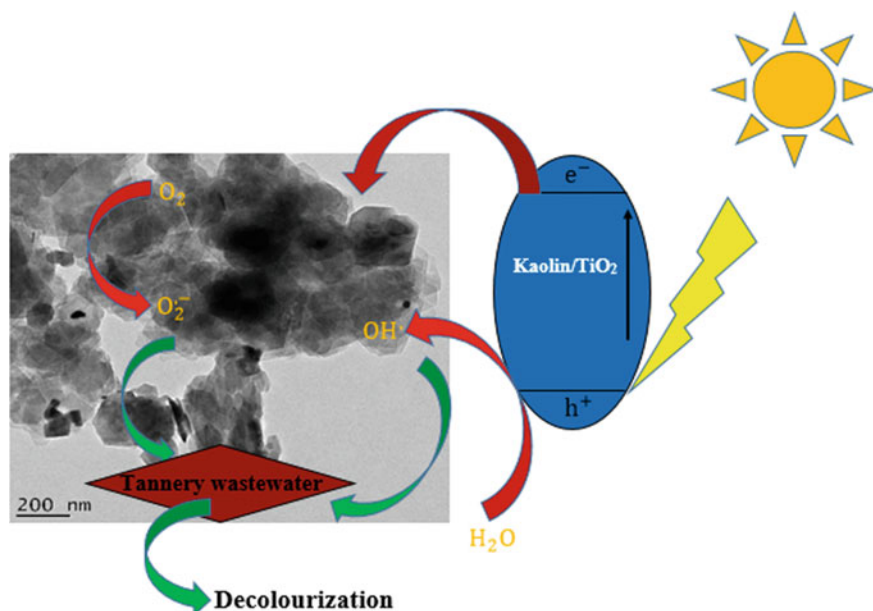


**Fig. 13** The proposed mechanism of decolourization of tannery wastewater

where  $k_{app}$  is the apparent first-order rate constant ( $\text{min}^{-1}$ ),  $C_o$  and  $C_t$  are the concentration of the pollutants at times 0 and  $t$ , respectively. The  $k_{app}$  values for COD and TOC degradation were calculated by plotting  $\ln \frac{C_o}{C_t}$  against time ( $t$ ) (see Figs. 14 and 15) and presented in Table 2.

The correlation coefficient ( $R^2$ ) of the studies were greater than 0.98, indicating the difference between  $R^2$  values and adjusted values less than 0.2. This revealed that the photodegradation of COD and TOC using kaolin/TiO<sub>2</sub> fitted well for apparent first-order kinetics. This observation corresponds to the finding of Hadjtaief et al. (2017).

### 3.2 Reusability Study

The stability of kaolin/TiO<sub>2</sub> was evaluated efficiently at optimum conditions for six cycles, and the results are depicted in Fig. 16. During cycles 1 to 3 of the photocatalyst, there was no significant change in the activities of the catalyst in terms of discolouration, removal of TOC and COD. However, the photocatalyst loses its removal efficiencies from the cycle. These results showed that kaolin/TiO<sub>2</sub> had easy and good recyclability.

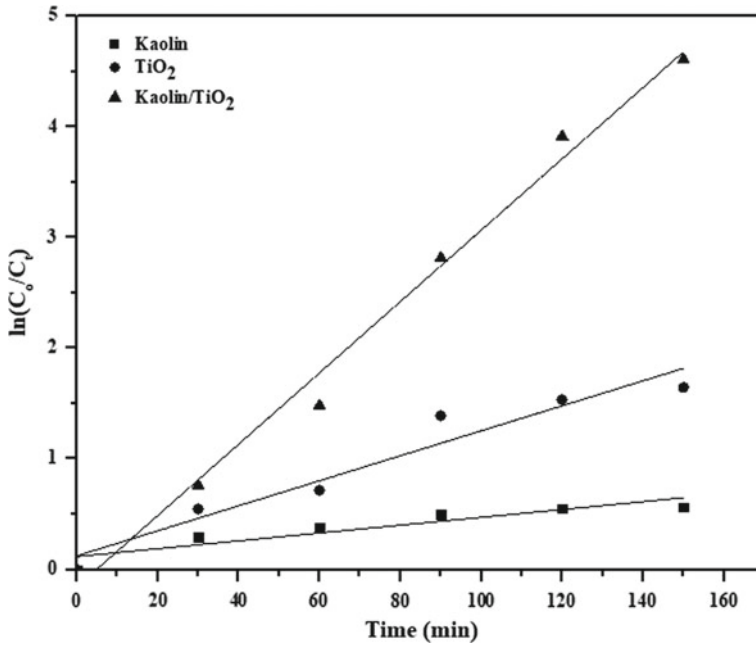


Fig. 14 The reaction kinetics for TOC removal in tannery wastewater

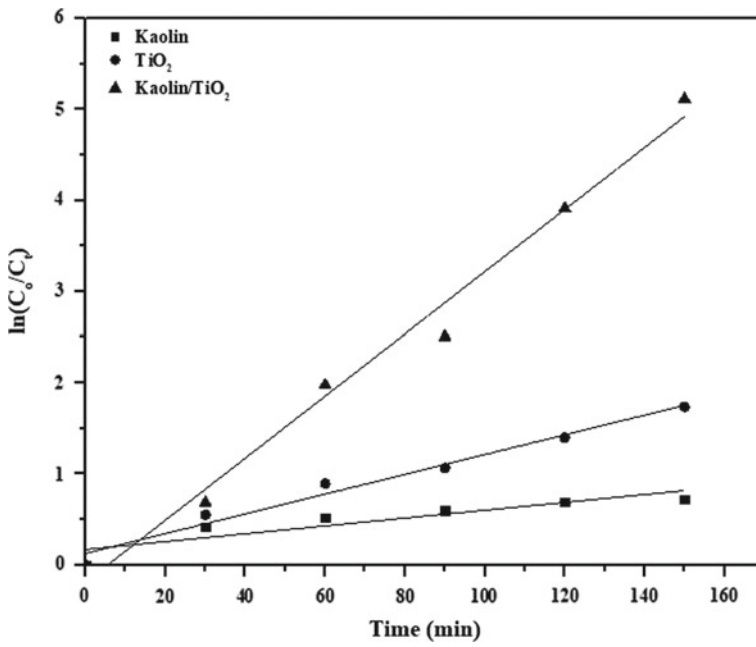
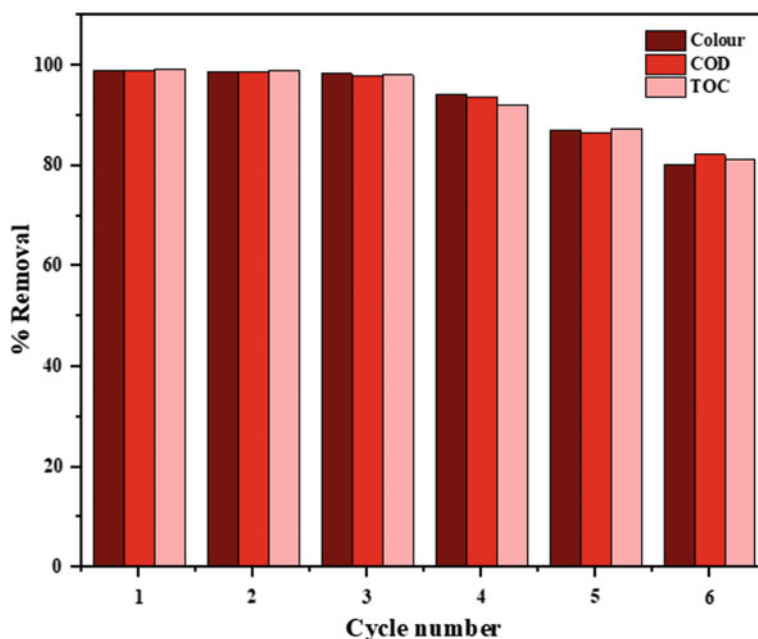


Fig. 15 The reaction kinetics for BOD removal in tannery wastewater

**Table 2** Pseudo-first-order kinetic parameters for TOC and BOD removal

Parameter	Sample	$k_{app}$	$R^2$	Adjusted $R^2$
TOC	Kaolin	0.00354	0.92499	0.81951
	TiO <sub>2</sub>	0.01129	0.97034	0.92695
	Kaolin/TiO <sub>2</sub>	0.03221	0.99493	0.98735
BOD	Kaolin	0.00431	0.90841	0.78151
	TiO <sub>2</sub>	0.01066	0.98892	0.97245
	Kaolin/TiO <sub>2</sub>	0.0346	0.99329	0.98327

**Fig. 16** Photocatalysis reuse cycle for removal of colour, COD and TOC in tannery wastewater

## 4 Conclusions

The present study investigated the removal of COD and TOC in tannery wastewater under sunlight using kaolin, TiO<sub>2</sub> and kaolin/TiO<sub>2</sub>. The nanoadsorbents were prepared using the sol-gel method and characterized using HRSEM, Raman spectroscopy, HRTEM-EDX and SAED, EDX. TEM and EDX confirmed the presence of TiO<sub>2</sub>. The kaolin, TiO<sub>2</sub> and kaolin/TiO<sub>2</sub> were used to remove TOC and BOD in tannery wastewater. The removal efficiencies were found to be time and dosage-dependent. Almost a complete decolourization of tannery wastewater within 90 min under sunlight in the presence of kaolin/TiO<sub>2</sub> nanocomposites is confirmed. This

performance could be attributed to the synergistic between kaolin and TiO<sub>2</sub>. The possible mechanism of discolouration of tannery wastewater was also discussed. The results indicate the feasibility of using kaolin/TiO<sub>2</sub> offer a new nanoadsorbent for water purification processes and photocatalytic discolourization of organic pollutants by natural solar radiations.

**Declaration of Competing Interest** The authors report no declarations of interest.

## References

- Ahmed S, Khan FSA, Mubarak NM, Khalid M, Tan YH, Mazari SA, Karri RR, Abdullah EC (2021) Emerging pollutants and their removal using visible-light responsive photocatalysis—a comprehensive review. *J Environ Chem Eng* 9(6)
- Aliou Guillaume PL, Chelaru AM, Visa M, Lassine O (2018) Titanium Oxide-Clay as adsorbent and photocatalysts for wastewater treatment. *J Membr Sci Technol* 08(01)
- Blanco-Vargas A, Ramírez-Sierra CF, Duarte-Castañeda M, Beltrán-Villarraga M, Medina-Córdoba LK, Florido-Cuellar AE, Cardona-Bedoya JA, Campos-Pinilla C, Pedroza-Rodríguez AM (2018) A novel textile wastewater treatment using ligninolytic co-culture and photocatalysis with TiO<sub>2</sub>. *Univ Sci* 23(3):437–464
- Boruah A, Rasheed A, Mendhe VA, Ganapathi S (2019) Specific surface area and pore size distribution in gas shales of Raniganj Basin, India. *J Petroleum Explor Produc Technol* 9(2):1041–1050
- Crini G, Lichtfouse E (2019) Advantages and disadvantages of techniques used for wastewater treatment. *Environ Chem Letters* 17(1):145–155
- de Araujo Scharnberg AR, de Loreto AC, Wermuth TB, Alves AK, Arcaro S, dos Santos PAM, Rodriguez ADAL (2020) Porous ceramic supported TiO<sub>2</sub> nanoparticles: enhanced photocatalytic activity for Rhodamine B degradation. *Boletín De La Sociedad Española De Cerámica y Vidrio* 59(6):230–238
- Dehghani MH, Omrani GA, Karri RR (2021) Solid Waste—sources, toxicity, and their consequences to human health. In *Soft computing techniques in solid waste and wastewater management*. Elsevier, pp 205–213. <https://doi.org/10.1016/B978-0-12-824463-0.00013-6>
- Dukic AB, Kumrić KR, Vukelić NS, Stojanović ZS, Stojmenović MD, Milošević SS, Matović LL (2015) Influence of ageing of milled clay and its composite with TiO<sub>2</sub> on the heavy metal adsorption characteristics. *Ceram Int* 41(3):5129–5137
- Engwa GA, Ferdinand PU, Nwalo FN, Unachukwu MN (2019) Mechanism and health effects of heavy metal toxicity in humans. In *Poisoning in the modern world—new tricks for an old dog?* IntechOpen.
- Gilja V, Novaković K, Travas-Sejdic J, Hrnjak-Murčić Z, Kraljić Roković M, Žic M (2017) Stability and synergistic effect of polyaniline/TiO<sub>2</sub> photocatalysts in degradation of azo dye in wastewater. *Nanomaterials* 7(12):412
- Hadjltaief HB, Zina MB, Galvez ME, Costa PD (2017) Photocatalytic degradation of methyl green dye in aqueous solution over natural clay-supported ZnO-TiO<sub>2</sub> catalysts. *J Photochem Photobiol A: Chem* 315:25–33
- Hadjltaief HB, Ameer SB, Da Costa P, Zina MB, Galvez ME (2018) Photocatalytic decolorization of cationic and anionic dyes over ZnO nanoparticle immobilized on natural Tunisian clay. *Appl Clay Sci* 152:148–157
- Hadjltaief HB, Gálvez ME, Zina MB, Da Costa P (2019) TiO<sub>2</sub>/clay as a heterogeneous catalyst in photocatalytic/photochemical oxidation of anionic reactive blue 19. *Arab J Chem* 12(7):1454–1462

- Karri RR, Ravindran G, Dehghani MH (2021) Wastewater—sources, toxicity, and their consequences to human health. In *Soft computing techniques in solid waste and wastewater management*. Elsevier, pp 3–33. <https://doi.org/10.1016/B978-0-12-824463-0.00001-X>
- Khan FSA, Mubarak NM, Khalid M, Tan YH, Abdullah EC, Rahman ME, Karri RR (2021) A comprehensive review on micropollutants removal using carbon nanotubes-based adsorbents and membranes. *J Environ Chem Eng* 9(6)
- Laysandr aL, Sari MWMK, Soetaredjo FE, Foe K, Putro JN, Kurniawan A, Ju Y, Ismadji S (2017) Adsorption and photocatalytic performance of bentonite-titanium dioxide composites for methylene blue and rhodamine B decoloration. *Heliyon* 3(12):e00488
- Lingamdinne LP, Choi JS, Angaru GKR, Karri RR, Yang JK, Chang YY, Koduru JR (2022) Magnetic-watermelon rinds biochar for uranium-contaminated water treatment using an electromagnetic semi-batch column with removal mechanistic investigations. *Chemosphere* 286
- Mahvi AH, Ghanbarian M, Nasser S, Khairi A (2009) Mineralization and discoloration of textile wastewater by TiO<sub>2</sub> nanoparticles. *Desalination* 239(1–3):309–316
- Manivannan R, Ryu J, Son YA (2021) Photo discoloration of eosin yellow dye under visible light using TiO<sub>2</sub>@ TPPS nanocomposite synthesized via ultrasonic assisted method. *Colloids Surf A Physicochem Eng Asp* 608:125601
- Mehmood A, Khan FSA, Mubarak NM, Tan YH, Karri RR, Khalid M, Walvekar R, Abdullah EC, Nizamuddin S, Mazari SA (2021) Magnetic nanocomposites for sustainable water purification—a comprehensive review. *Environ Sci Pollut Res* 28(16):19563–19588
- Mishra A, Mehtav A, Sharma M, Basu S (2017) Enhanced heterogeneous photodegradation of VOC and dye using microwave synthesized TiO<sub>2</sub>/Clay nanocomposites: a comparison study of different type of clays. *J Alloys Compd* 694:574–580
- Nabbou N, Belhachemi M, Boumelik M, Merzougui T, Lahcene D, Harek Y, Zorpas AA, Jeguirim M (2019) Removal of fluoride from groundwater using natural clay (kaolinite): optimization of adsorption conditions. *Comptes Rendus Chimie* 22(2–3):105–112
- Retamoso C, Escalona N, González M, Barrientos L, Allende-González P, Stancovich S, Serpell R, Fierro JLG, Lopez M (2019) Effect of particle size on the photocatalytic activity of modified rutile sand (TiO<sub>2</sub>) for the discoloration of methylene blue in water. *J Photochem Photobiol, A* 378:136–141
- Rodrigues M, Souza AG, Santos IMG (2016) Brazilian kaolin wastes: synthesis of zeolite P at low-temperature. *Am Chem Sci J* 12(4):1–11
- Silvestri S, Foletto EL (2017) Preparation and characterization of Fe<sub>2</sub>O<sub>3</sub>/TiO<sub>2</sub>/clay plates and their use as photocatalysts. *Ceram Int* 43(16):14057–14062
- Silvestri S, Stefanello N, Sulkovski AA, Foletto EL (2020) Preparation of TiO<sub>2</sub> supported on MDF biochar for simultaneous removal of methylene blue by adsorption and photocatalysis. *J Chem Technol Biotechnol* 95(10):2723–2729
- Wang C, Shi H, Zhang P, Li Y (2011) Synthesis and characterization of kaolinite/TiO<sub>2</sub> nano-photocatalysts. *Appl Clay Sci* 53(4):646–649
- Yang C, Zhu Y, Wang J, Li Z, Su X, Niu C (2015) Hydrothermal synthesis of TiO<sub>2</sub>-WO<sub>3</sub>-bentonite composites: Conventional versus ultrasonic pretreatments and their adsorption of methylene blue. *Appl Clay Sci* 105–106:243–251